Deep–Sea Research I 160 (2020) 103263

Contents lists available at ScienceDirect

Deep-Sea Research Part I

journal homepage: http://www.elsevier.com/locate/dsri

Effects of phytoplankton community composition and productivity on sea surface pCO_2 variations in the Southern Ocean

Shintaro Takao [a,b,*], Shin-Ichiro Nakaoka [a], Fuminori Hashihama [c], Keishi Shimada [c], Hisayuki Yoshikawa-Inoue [b], Toru Hirawake [d], Jota Kanda [c], Gen Hashida [e], Koji Suzuki [b]

[a] National Institute for Environmental Studies, 16-2 Onogawa, Tsukuba, Ibaraki, 305-8506, Japan
[b] Faculty of Environmental Earth Science, Hokkaido University, North 10 West 5, Kita-ku, Sapporo, Hokkaido, 060-0810, Japan
[c] Tokyo University of Marine Science and Technology, 4-5-7 Konan, Minato-ku, Tokyo, 108-8477, Japan
[d] Faculty of Fisheries Sciences, Hokkaido University, 3-1-1 Minato-cho, Hakodate, Hokkaido, 041-8611, Japan
[e] National Institute of Polar Research, 10-3 Midori-cho, Tachikawa, Tokyo, 190-8518, Japan

ARTICLE INFO

Keywords:
Phytoplankton community composition
Diatoms
Southern Ocean
Net primary productivity
Carbon dioxide

ABSTRACT

The Southern Ocean is a vast net sink for atmospheric carbon dioxide (CO_2), with marine phytoplankton playing a crucial role in CO_2 fixation. We assessed how changes in the dominant phytoplankton community and net primary productivity (NPP) affected variations in the partial pressure of CO_2 in surface water (pCO_2^{sw}) in the Indian sector of the Southern Ocean during austral summer. pCO_2^{sw} was negatively correlated with total phytoplankton and diatom abundances, as estimated from pigment signatures, in the zone south of the Antarctic Circumpolar Current; however, pCO_2^{sw} was not correlated with haptophyte abundance. Additionally, a stronger correlation was found between pCO_2^{sw} and total phytoplankton NPP than between chlorophyll *a* concentration and pCO_2^{sw}. We reconstructed pCO_2^{sw} at inter-annual scale using satellite data and assessed the inter-annual variability of air-sea CO_2 flux. Over the period from 1997 to 2007, the integrated CO_2 fluxes over the study region showed very large variations from a small source to a strong sink. Variations in the integrated CO_2 fluxes were also correlated with changes in satellite-derived phytoplankton community in the Indian sector of the Southern Ocean and changes in the dominant phytoplankton community may control CO_2 dynamics in the marginal ice zone.

1. Introduction

The Southern Ocean is one of the most important regions for the global carbon cycle, as it is a vast net sink for atmospheric carbon dioxide (CO_2) (e.g., Landschützer et al., 2015; Lenton et al., 2013; McNeil et al., 2007), and thus can absorb a large amount of anthropogenic CO_2 (Gruber et al., 2009; Khatiwala et al., 2009; Ito et al., 2010; Mikaloff Fletcher et al., 2006). During the austral summer in particular, phytoplankton productivity plays a crucial role in the carbon cycle of the Southern Ocean (e.g., Metzl et al., 2006; Takahashi et al., 2012). In the zone south of the Antarctic Circumpolar Current (SACCZ) in the Indian sector of the Southern Ocean, Takao et al. (2012) demonstrated that changes in net primary productivity (NPP) were strongly affected by the dominant members of the phytoplankton community using satellite remote sensing data. The transport efficiency of particulate organic carbon (POC) from the surface to deeper waters (i.e., the biological carbon pump) is strongly dependent on the composition of the phytoplankton community (e.g., Tréguer et al., 2018). Diatoms, which account for approximately 40% of annual NPP in the global ocean (Nelson et al., 1995), are one of the main contributors to the global carbon cycle. Large diatoms in particular appear to increase the efficiency of the biological carbon pump due to their heavy silica frustules (e.g., Tréguer and Pondaven, 2000). Coccolithophores, which belong to the division Haptophyta, also seem to play an important role in the regulation of atmospheric CO_2. Precipitation of calcium carbonate ($CaCO_3$) by coccolithophores ($Ca^{2+} + 2HCO_3^- \Leftrightarrow CaCO_3 + CO_2 + H_2O$) increases CO_2 concentrations in the surrounding seawater and is a potential source of CO_2 from the ocean to the atmosphere (Frankignoulle et al., 1994), whereas carbonate also increases sinking velocities and thus particle export to the deep ocean (e.g., Armstrong et al., 2002; Buitenhuis et al., 2001). On the other hand, the non-calcifying haptophyte *Phaeocystis antarctica* regularly forms huge colonies with high sinking rates in

* Corresponding author.
E-mail address: takao.shintaro@nies.go.jp (S. Takao).

https://doi.org/10.1016/j.dsr.2020.103263
Received 4 September 2019; Received in revised form 11 March 2020; Accepted 11 March 2020
Available online 19 March 2020

seasonal ice zones and coastal Antarctic waters, resulting in significant POC export from surface waters (DiTullio et al., 2000).

The dominant phytoplankton community is affected by long-term climate change in the Southern Ocean. For example, in coastal waters along the western shelf of the Antarctic Peninsula (WAP), which has been the most rapidly warming region on earth over the past 50 years (e.g., Turner et al., 2005), greater dominance of cryptophytes over diatoms has occurred, which is hypothesized to be a response to regional warming (Moline et al., 2004). Montes-Hugo et al. (2009) found a significant change in chlorophyll *a* (chl *a*) concentrations over the past 30 years (1978–2006) along the WAP based on satellite and field data. This change could be accompanied by changes in the dominant phytoplankton community associated with rapid regional climate change along the WAP. More recently, Brown et al. (2019) found a nearly fivefold increase in summer oceanic CO_2 uptake over the past 25 years (1993–2017) along the WAP with greater upper ocean stability and changes in phytoplankton dynamics (i.e., biomass and community composition), which is affected by changes in wind, sea ice and meltwater dynamics, driven by regionally specific climatic variations, such as the Southern Annular Mode (SAM). The links between regionally specific climatic variations and satellite-derived dominant phytoplankton communities and NPP data were also examined. Alvain et al. (2013) observed large-scale shifts in the dominance of diatoms, with larger anomalies during extreme positive periods of the SAM in the Southern Ocean. In the Indian sector of the marginal ice zone (65–70°S), Johnston and Gabric (2011) found a significant positive correlation between summer NPP and the SAM index over the previous decade (1997–2007).

Several studies have reported an influence of phytoplankton biomass, as measured through chl *a* concentration, on pCO_2^{sw} variations in the Southern Ocean (e.g., Carrillo et al., 2004; Jabaud-Jan et al., 2004; Metzl et al., 2006; Nomura et al., 2014; Stoll et al., 2002). In the Indian sector, Jabaud-Jan et al. (2004) reported a strong oceanic CO_2 sink associated with a significant decrease in surface silicic acid concentration, suggesting that a large diatom bloom had occurred. However, few studies have explored the relationship between phytoplankton community composition and pCO_2^{sw} in the Southern Ocean. Moreau et al. (2012) investigated the influence of phytoplankton community composition on variations in the difference between atmospheric and sea surface pCO_2 (ΔpCO_2) near the WAP. The authors found a significant negative correlation between chl *a* concentration and ΔpCO_2 at stations dominated by diatoms, but not at those dominated by phytoflagellates. The enhanced oceanic CO_2 uptake along the WAP over the past 25 years as mentioned above could be associated with shifts in phytoplankton community composition, as there has been a large significant increase in diatoms with higher ΔpCO_2 values relative to cryptophytes with lower ΔpCO_2 values at a similarly shallow mixed layer condition (Brown et al., 2019). In the Weddell Sea, Moreau et al. (2013) reported significant negative correlations between carbon biomass of both diatoms and phytoflagellates and ΔpCO_2. These results suggest that phytoplankton community composition plays a crucial role in the relationship between chl *a* concentration or carbon biomass and CO_2 dynamics, although previous studies have been limited to waters along the WAP and in the Weddell Sea. Thus, assessing how changes in the abundance and productivity of the phytoplankton community affect changes in pCO_2^{sw} in other regions of the Southern Ocean is crucial. The objective of this study was to determine how changes in the phytoplankton community and NPP affect pCO_2^{sw} levels in the Indian sector of the SACCZ and how this impact inter-annual integrated air-sea CO_2 fluxes in this region.

2. Materials and methods

2.1. Sampling procedures and hydrographic measurements

Samples were collected to measure NPP, phytoplankton community composition, macronutrients, and pCO_2^{sw} in the Indian Sector of the Southern Ocean during three cruises of the TR/V *Umitaka-Maru* (Tokyo University of Marine Science and Technology) during the austral summers of 2005/2006, 2007/2008, and 2008/2009. During these cruises, 11 stations in the SACCZ (Fig. 1) were found that exhibited a temperature minimum (T_{min}) layer, thought to be the remnant of the mixed layer from the previous late winter. Its properties were used as proxies for those of the winter mixed layer (e.g., Ishii et al., 1998, 2002; Jennings et al., 1984). In this study, same sampling procedures and sensors for hydrographic measurements were used throughout the three cruises.

Vertical profiles of water temperature and salinity at each station were obtained with a CTD system (SBE 9plus, Sea-Bird Electronics, Inc.) that simultaneously measures seawater conductivity, temperature, and pressure (depth). Pre-cruise calibrations were performed for the conductivity, temperature, and pressure sensors at Sea-Bird Electronics, Inc. The accuracy of temperature and conductivity is ±0.001 °C and ±0.0003 S/m, respectively. Conductivity was converted to salinity using the SBE Data Processing software, and sensor salinity was corrected by the value of bottle salinity taken from several depths at some stations. To identify observational data in the SACCZ, the position of the Southern Boundary of the Antarctic Circumpolar Current during each cruise was located using vertical profiles of water temperature and salinity obtained with the CTD system, following the criteria of Orsi et al. (1995). The mixed layer depth (MLD) at each station was determined from vertical profiles of water temperature. In this study, the MLD was defined as the depth at which the change from a near-surface value at 10 m depth was 0.2 °C (de Boyer Montégut et al., 2004; Dong et al., 2008).

Samples for NPP and phytoplankton community composition in surface waters were collected from approximately 1–5 m depth using Teflon-coated Niskin bottles attached to a CTD system (ICTD, Falmouth Scientific Inc.). To obtain depth-integrated NPP, seawater samples were collected at several depths above the euphotic layer depth, which is defined as the depth at which photosynthetically available radiation (PAR) is 1% of its surface level. Samples for macronutrients, including nitrite plus nitrate (hereafter referred to as nitrate), phosphate, and silicic acid, were collected at several depths from the surface to bottom using the Niskin bottles attached to the SBE CTD system. Macronutrients were analyzed at an onshore laboratory (samples from 2005/2006) or onboard the ship (samples from 2007/2008 and 2008/2009) with a Bran + Luebbe autoanalyzer (AACS-III) following the manufacturer's protocol. The analytical precision (coefficient of variation) was 1.1% at 20 mmol m^{-3} nitrate, 2.1% at 2 mmol m^{-3} phosphate, and 0.8% at 80 mmol m^{-3} silicic acid.

The surface seawater temperature and salinity were measured continuously with a temperature sensor (DS103, Tateyama Kagaku High-Technologies Co.) and a conductivity sensor (Excell Thermosalinograph, Falmouth Scientific Inc.) along cruise tracks using seawater that drew from the bottom of the ship (approximately 5 m below the sea surface). During the three cruises, the accuracy of temperature and salinity is ±0.02 °C and ±0.03, respectively.

In vivo fluorescence at sea surface was measured continuously with a fluorescence sensor (WETStar, WETLabs Inc.). Sea surface chl *a* concentration was estimated from the fluorescence value based on the relationships among fluorescence, chl *a* concentration, and PAR measured in the same time. Total chl *a* concentration was determined with a Turner Designs fluorometer (Model 10-AU) using the non-acidification method of Welschmeyer (1994). Sea surface PAR was measured with an air quantum sensor (LI-190SB, LI. COR Inc.).

2.2. pCO_2 measurements

Atmospheric pCO_2 (pCO_2^{air}) and pCO_2^{sw} were measured semi-continuously using a system similar to that described by Inoue et al. (1995, 1999) for the 2005/2006 cruise and a system similar to that described by Murphy et al. (2001) for the 2007/2008 and 2008/2009 cruises. Uncontaminated seawater was collected from a sea chest onboard the ship and introduced into an equilibrator at approximately 10

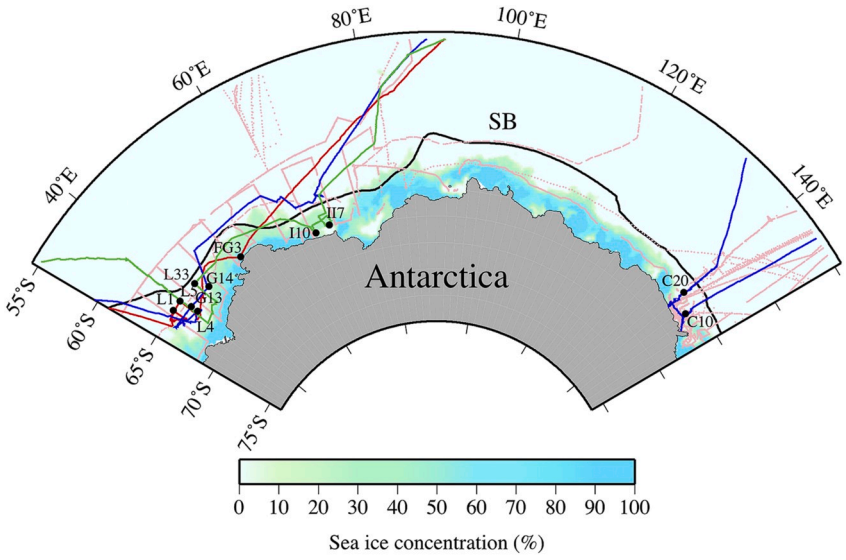

Fig. 1. Locations of sampling stations in the zone south of the Antarctic Circumpolar Current (SACCZ) in the Indian sector of the Southern Ocean. Closed circles indicate stations where seawater was sampled. Red, blue, and green lines represent the cruise tracks followed in 2005/2006, 2007/2008, and 2008/2009, respectively. Pink dots indicate locations of the Surface Ocean CO_2 Atlas (SOCAT) version 2019 data (1997/1998–2006/2007 during summer) using this study. The satellite image of sea ice concentration was derived by averaging 11 AMSR-E daily images from the water sampling date shown in Table 1. The black line represents the climatological location of the Southern Boundary of the Antarctic Circumpolar Current (SB) reported by Orsi et al. (1995). (For interpretation of the references to color in this figure legend, the reader is referred to the Web version of this article.)

L min^{-1}. An aliquot of sampled air equilibrated with seawater was introduced into a non-dispersive infrared gas analyzer after removing water vapor. Ambient air was collected from an inlet on the bow side of the ship to measure pCO_2^{air}. The effect of increasing seawater temperature on the measured value of pCO_2^{sw} was corrected using the temperature difference between the sea surface and the equilibrator and the iso-chemical temperature dependence of pCO_2^{sw} reported by Copin--Montégut (1988, 1989). The CO_2 measurement system was calibrated at 12-h intervals using four air-based standard gases with CO_2 concentrations of 200–400 ppm based on the World Meteorological Organization (WMO) mole fraction scale. Atmospheric pressure data recorded onboard the ship were used to calculate pCO_2^{sw} and pCO_2^{air} from the measured CO_2 concentrations. The overall uncertainty of pCO_2^{sw} measurements was estimated as approximately 3 µatm. The value of pCO_2^{sw} at each station was averaged over 10-min intervals, which included the time of water sampling.

In this study, we used the fugacity of CO_2 (fCO_2) in surface water obtained from the Surface Ocean CO_2 Atlas (SOCAT) version 2019 database (Bakker et al., 2016) as independent pCO_2^{sw} measurements. Cruises of SOCAT data used in this study are listed in Table S1.

2.3. Net primary productivity and phytoplankton pigment analysis

Seawater samples (0.5–1 L) collected for NPP analysis were dispensed into acid-cleaned polycarbonate bottles and inoculated with a solution of $NaH^{13}CO_3$ (99 atom% ^{13}C, Shoko Co., Ltd.) equivalent to approximately 10% of the dissolved inorganic carbon (DIC) in seawater. The bottles were incubated under natural light for 24 h in an on-deck incubator. The temperature in the incubator was maintained using surface seawater pumped from the bottom of the ship. Photosynthetic rates were calculated according to the method of Hama et al. (1983). A detailed description of the sample analysis procedure is provided in Hirawake et al. (2011).

Seawater samples (0.5–7 L) for phytoplankton pigment analyses were filtered onto 25-mm Whatman GF/F filters. The filters were blotted and stored in liquid nitrogen or a freezer at −80 °C prior to analysis on land. The analytical procedure used for pigments samples is detailed in Hashihama et al. (2008). In this study, surface pigment samples taken from 1 to 5 m depth were interpreted using the matrix factorization program CHEMTAX (Mackey et al., 1996) to estimate the contributions of each algal class to total chl *a*, as determined using a high-performance liquid chromatography (HPLC) system. The CHEMTAX calculations were described in detail by Takao et al. (2012).

2.4. Seasonally integrated net community production

To assess the effects of biological activities on the CO_2 system in seawater from the beginning of spring until our observation period, seasonally integrated net community production (NCP), defined as NPP minus respiration by all heterotrophic organisms in the water column (Codispoti et al., 1986; Minas et al., 1986), was estimated from the deficit of macronutrients in the surface layer compared to the remnant of the winter mixed layer (e.g., Hoppema et al., 1999; Jennings et al., 1984; Shim et al., 2006). Sweeney et al. (2000) noted relatively constant carbon/nitrate (C/N) ratios among phytoplankton species. In the Indian sector of the Southern Ocean, Ishii et al. (1998, 2002) reported that the C/N ratios of composite plots in the marginal ice zone were 6.2–6.3. Therefore, NCP in this study was estimated from the deficit of nitrate (ΔN) and the classical Redfield ratio (i.e., C/N = 6.6; Redfield et al., 1963).

3. Results and discussion

3.1. Hydrography and pCO_2^{sw}

Hydrographic conditions and CO_2 values at each station are listed in Table 1. Sea surface temperature (SST) ranged from −0.9 °C at Stn. FG3 to 1.5 °C at Stn. II7, and sea surface salinity (SSS) ranged from 32.7 at Stn. II7 to 33.9 at Stn. FG3. pCO_2^{sw} at each station varied widely, from 205 µatm at Stn. II7 to 391 µatm at Stn. L33, and pCO_2^{sw} along the cruise tracks in the region south of 60°S ranged from 191 to 424 µatm (Fig. 2a), which was correspondent with the range reported by SOCAT version 2019 (i.e., 179–405 µatm) in the same region during the austral summers (December–February) of 2005/2006, 2007/2008, and 2008/2009 (Bakker et al., 2016). Atmospheric CO_2 mole fraction (xCO_2^{air}) at each station ranged from 378 to 387 ppm (Table 1), and a mean xCO_2^{air} along the cruise tracks was 378 ± 1, 383 ± 1, and 385 ± 1 ppm for the 2005/2006, 2007/2008, and 2008/2009 cruise, respectively, with a slightly higher value measured at the Syowa monitoring station (69.01°S, 39.59°E) near the study region (i.e., 378, 382, and 384 ppm, respectively) during the same periods (http://www.esrl.noaa.gov/gmd/dv/iadv/). pCO_2^{air} at each station varied from 360 µatm at Stn. FG3 to 376 µatm at Stns. L33, and pCO_2^{air} along the cruise tracks ranged from 358 to 380 µatm (Fig. 2a). Although this variation was related to changes in atmospheric pressure in our study region, the variation of pCO_2^{air} along the cruises tracks was much smaller than that of pCO_2^{sw} (Fig. 2a).

Table 1
Summary of data from each station. SST, sea surface temperature (°C); SSS, sea surface salinity; pCO_2^{sw}, sea surface pCO_2 (μatm); pCO_2^{air}, atmospheric pCO_2 (μatm); xCO_2^{air}, atmospheric CO_2 mole fraction (ppm); ΔSi/ΔN, deficit ratio of silicic acid to nitrate in the water column; PP_{eu}, depth-integrated NPP (mg C m^{-2} d^{-1}) within the euphotic layer; NCP, seasonally integrated net community production (g C m^{-2} $season^{-1}$).

Cruise	Station	Date	Latitude	Longitude	SST	SSS	pCO_2^{sw}	pCO_2^{air}	xCO_2^{air}	ΔSi/ΔN	PP_{eu}	NCP
			(°S)	(°E)	(°C)		(μatm)	(μatm)	(ppm)		(mg C m^{-2} d^{-1})	(g C m^{-2} $season^{-1}$)
UM0506	L1	13 Jan 2006	65.0	36.0	−0.4	33.6	372	370	381	1.4	224	2
UM0506	L5	14 Jan 2006	65.0	38.0	−0.1	33.8	366	369	378	2.1	184	6
UM0506	FG3	19 Jan 2006	65.9	51.3	−0.9	33.9	317	360	378	1.1	976	41
UM0708	L4	31 Dec 2007	66.5	38.5	−0.7	33.7	316	372	382	2.2	677	13
UM0708	G13	4 Jan 2008	65.9	38.5	−0.2	33.5	284	368	384	2.4	1003	20
UM0708	G14	5 Jan 2008	65.9	43.3	−0.7	33.9	354	368	382	2.5	298	16
UM0708	C20	2 Feb 2008	65.1	139.8	0.4	33.7	378	369	383	8.6	158	8
UM0708	C10	11 Feb 2008	66.0	143.0	−0.8	33.8	335	365	384	4.3	171	45
UM0809	L33	19 Jan 2009	65.0	42.0	0.6	33.7	391	376	386	4.1	327	4
UM0809	I10	23 Jan 2009	67.3	65.9	1.2	33.0	255	374	387	0.1	1484	63
UM0809	II7	25 Jan 2009	67.2	68.8	1.5	32.7	205	370	385	1.0	1499	35

The values of SST, SSS, and chl *a* concentration along the cruise tracks varied widely in the region south of 60°S (Fig. 2b–d). In areas west of 80°E, relatively high (low) pCO_2^{sw} was observed with low (high) chl *a* concentrations and relatively constant SST, indicating that biological processes control the distribution of pCO_2^{sw} (e.g., Jabaud-Jan et al., 2004; Stoll et al., 2002). High chl *a* concentrations were observed with relatively low SSS near the sea ice edge in the areas around 40°E and 70°E (Stns. I10 and II7). Values of pCO_2^{sw}, SST, and SSS in areas east of 140°E changed gradually from north to south. The highest pCO_2^{sw} values were observed along the 140°E transect, with relatively low chl *a* concentration and high SST, indicating that thermodynamic processes control the distribution of pCO_2^{sw} (e.g., Takahashi et al., 1997).

At 7 of 11 stations, potential temperature and salinity diagrams indicated clear T_{min} layers (black dashed box in Fig. 3). At station FG3, near the coast of Antarctica where the MLD was deeper than 100 m, a T_{min} layer was found near the bottom (i.e., 239 m). Compared to other stations, the sea ice minimum occurred more than 1 month later at station FG3 (Nomura et al., 2014). Thus, weaker thermal stratification at station FG3 may be caused by slow sea ice retreat. At three other stations (C10, I10, and II7), the water masses present included Antarctic surface water (ASW), modified circumpolar deep water (mCDW), and modified shelf water (mSW), which was formed from vertical mixing of shelf water with mCDW (e.g., Orsi and Wiederwohl, 2009; Williams et al., 2010). At these stations, T_{min} layers were observed within mSW, and no clear T_{min} layers were found with the water properties of the remnant mixed layer from the preceding late winter (winter water: WW), defined by potential temperature between −1.9 °C and −1.5 °C and salinity between 34.2 and 34.5 (Tomczak and Liefrink, 2005). In this study, the deficit ratio of silicic acid to nitrate (ΔSi/ΔN) in the water column from the preceding winter to the observation time and seasonally integrated NCP were estimated using values of macronutrients measured in the T_{min} layers within the WW. The values of nitrate and silicic acid in T_{min} layers within the WW were 30.3 ± 1.2 mmol m^{-3} and 62.2 ± 7.0 mmol m^{-3} (n = 11), respectively. These values were comparable to climatological values of nitrate and silicic acid in August (30.7 ± 1.5 mmol m^{-3} and 60.5 ± 2.6 mmol m^{-3}) reported previously for the same region (Garcia et al., 2014).

3.2. Phytoplankton community composition and pCO_2^{sw}

Based on pigment signatures, diatoms and haptophytes contributed strongly to the surface chl *a* biomass, making up more than 80% of the phytoplankton community at most stations (Fig. 4). The contributions of diatoms to chl *a* biomass varied from 19 to 92%, with a mean of 53%. Type 8 haptophytes (presumably *Phaeocystis antarctica*; Zapata et al., 2004) were the second greatest contributors to chl *a* biomass, ranging from 0 to 72% (mean 21%). For ΔSi/ΔN in the water column, Sweeney et al. (2000) noted that a value greater than 1.0 indicates the predominance of diatoms, whereas a value less than 0.5 indicates the predominance of *P. antarctica*. However, macronutrient uptake ratios of phytoplankton are thought to change not only among species but also with environmental and physiological conditions (e.g., Arrigo et al., 1999). At 10 of 11 stations, ΔSi/ΔN values in the water column were greater than 1.0 (Table 1). These results suggest that diatoms may dominate phytoplankton assemblages in the water column from austral spring to summer, as well as during our observation periods.

Fig. 5 illustrates the relationships between pCO_2^{sw} and the surface chl *a* concentration for total phytoplankton, diatoms, and type 8 haptophytes. Surface chl *a* concentrations measured with HPLC ranged from 0.03 to 1.15 mg m^{-3} (Fig. 5a). The chl *a* concentrations for diatoms and type 8 haptophytes ranged from 0.01 to 0.57 mg m^{-3} (Fig. 5b) and 0–0.19 mg m^{-3} (Fig. 5c), respectively. In the SACCZ during our cruises, pCO_2^{sw} was negatively correlated with chl *a* concentrations for total phytoplankton ($r = -0.87$, $P < 0.001$, $n = 11$) and diatoms ($r = -0.75$, $P < 0.01$, $n = 11$) but not correlated with that for type 8 haptophytes (Fig. 5). Along the cruise tracks in the region south of 60°S, pCO_2^{sw} was also negatively correlated with the surface chl *a* concentration estimated from the fluorescence sensor, with a weaker linear relationship (i.e., gray dots in Fig. 5a). As noted above, Moreau et al. (2012) reported a significant negative correlation between chl *a* concentration and ΔpCO_2 at stations dominated by diatoms, but not at stations dominated by phytoflagellates during summer and fall in 3 consecutive years (i.e., 2002, 2003 and 2004) in coastal waters along the WAP. Using long-term records over the past 25 years (1993–2017), Brown et al. (2019) also reported a significant negative correlation between chl *a* concentration and ΔpCO_2 along the WAP. These findings are consistent with the results of the present study. We used pCO_2^{sw} rather than ΔpCO_2, and no significant differences were found between the results for pCO_2^{sw} and those for ΔpCO_2 (data not shown). On the other hand, Moreau et al. (2013) reported a significant negative correlation between the carbon biomass of phytoflagellates estimated using microscopy and ΔpCO_2 in the Weddell Sea. We did not observe such a trend in this study, although we estimated the abundance of each phytoplankton group using pigment signatures rather than microscopy. These results suggest that the effects of phytoplankton community composition on CO_2 dynamics may differ spatiotemporally within the Southern Ocean. Thus, further studies examining the relationship between pCO_2^{sw} and phytoplankton community composition in the Southern Ocean are needed.

3.3. Net primary productivity and pCO_2^{sw}

Fig. 6 shows the relationships of pCO_2^{sw} with surface NPP and depth-integrated NPP within the euphotic layer (PP_{eu}). Surface NPP ranged from 4.4 to 82.8 mg C m^{-3} day^{-1} (Fig. 6a). Similar to the relationship with the surface chl *a* concentration, pCO_2^{sw} was negatively correlated with surface NPP ($r = -0.90$, $P < 0.001$, $n = 11$). PP_{eu} ranged from 158

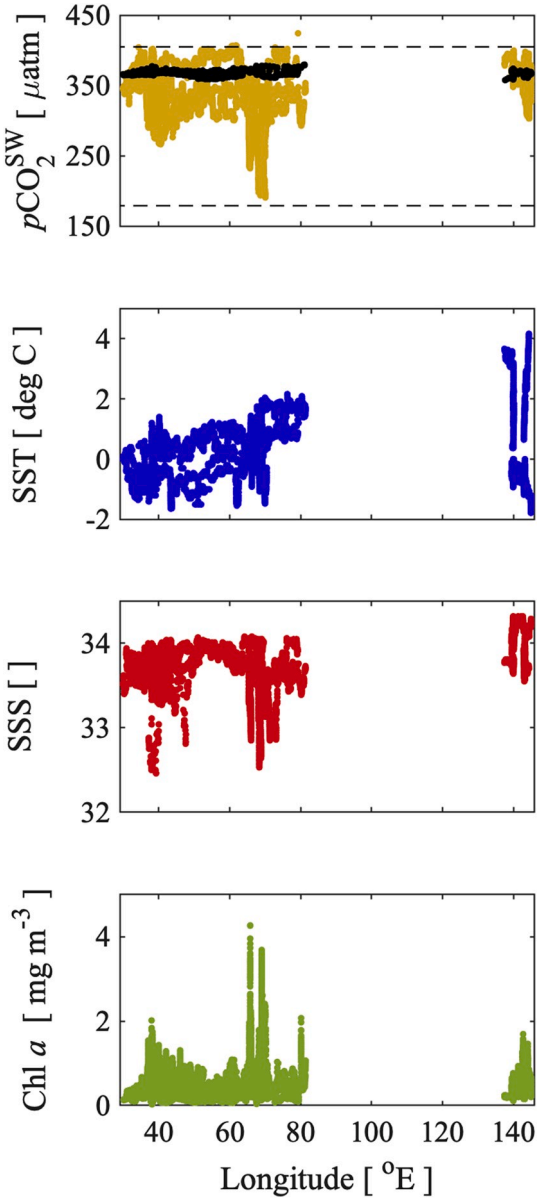

Fig. 2. Longitudinal distributions of (a) pCO_2^{sw} and pCO_2^{air} (black dots), (b) SST, (c) SSS, and (d) chl *a* concentration along the cruise tracks in the region south of 60°S shown in Fig. 1. Horizontal dashed lines in Fig. 2a represent the maximum and minimum value of pCO_2^{sw} reported by SOCAT version 2019 (Bakker et al., 2016) in the same region during our observation periods. Sea surface fCO_2 values from SOCAT were used as pCO_2^{sw}.

to 1499 mg C m^{-2} day^{-1} (Table 1) and was negatively correlated with pCO_2^{sw} ($r = -0.92$, $P < 0.001$, $n = 11$; Fig. 6b). Although NPP data for the Indian sector of the Southern Ocean are very limited, several studies have reported gross primary production (GPP) integrated throughout the water column in the area south of 60°S during austral spring to summer. Depth-integrated GPP was 301–4570 mg C m^{-2} day^{-1} along 30–80°E (Westwood et al., 2010), 125–890 mg C m^{-2} day^{-1} along 80–150°E (Strutton et al., 2000), and 49–895 mg C m^{-2} day^{-1} at 140°E (Yoshikawa et al., 2007). Goldman et al. (2015) reported a strong correlation between NPP and GPP values in the Southern Ocean based on ^{14}C incubations, with a slope of 0.61. Using this ratio with depth-integrated GPP values (i.e., 49–4570 mg C m^{-2} day^{-1}) reported in previous studies, estimated PP_{eu} varied from approx. 30 to 2790 mg C m^{-2} day^{-1}, and our PP_{eu} values of 158–1499 mg C m^{-2} day^{-1} fell within this range.

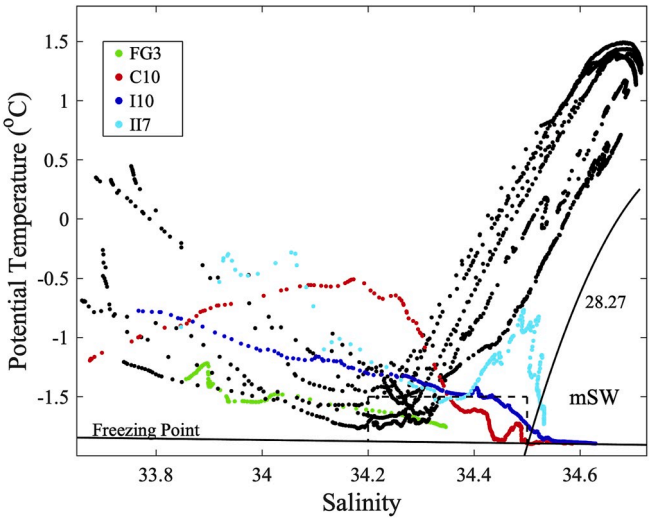

Fig. 3. Potential temperature and salinity diagram for sampling stations in water depths shallower than 500 m. Solid curve represents the 28.27 kg m^{-3} neutral density surface, horizontal line represents the freezing point of seawater, and black dashed box represents water properties of the remnant mixed layer from the preceding late winter (i.e., winter water).

The relationship between pCO_2^{sw} and PP_{eu} was consistent with that of surface NPP, and is expressed as follows:

$$pCO_2^{sw} = -0.1\ PP_{eu} + 389.8 \quad (1)$$

The relationships of pCO_2^{sw} with surface and depth-integrated NPP were slightly stronger than that between pCO_2^{sw} and surface chl *a* concentration (Tables 2 and 3).

Values of pCO_2^{sw} during our observation periods were affected by pCO_2^{sw} changes in physical and biological processes, especially from the beginning of austral spring into summer. As discussed in several studies (e.g., Moreau et al., 2012, 2013; Schloss et al., 2007; Shadwick et al., 2015), air-sea exchange of CO_2 is a process that occurs over a longer time scale (e.g., the residence time of CO_2 in the mixed layer ranges from several weeks to months) than the changes in biological factors such as phytoplankton abundance, composition and productivity analyzed in this study (i.e., hours). Seasonally integrated NCP ranged from 2 to 63 g C m^{-2} (Table 1); it was negatively correlated with pCO_2^{sw} ($r = -0.64$, $P < 0.05$, $n = 11$; Fig. 6c) and positively correlated with PP_{eu} ($r = 0.62$, $P < 0.05$, $n = 11$). These results suggest that CO_2 dynamics in the study region are driven mainly by biological activities, and the high phytoplankton abundance and productivity measured during our observation periods may have occurred continuously or intermittently from the beginning of austral spring to summer. Temporal changes in satellite chl *a* concentrations before the cruises would support this process. Relatively high satellite-derived chl *a* concentrations were observed before the cruises at stations with relatively high NCP (Table 1 and Fig. S1).

3.4. Estimation of pCO_2^{sw} distributions from satellite data

Previously, researchers estimated the distribution of pCO_2^{sw} using satellite images of chl *a* concentrations based on empirical relationships among in situ parameters, and reported that pCO_2^{sw} estimates incorporating chl *a* concentrations were more accurate in the North Pacific (e.g., Ono et al., 2004; Sarma et al., 2006) and the Southern Ocean (e.g., Xu et al., 2016). However, satellite-derived chl *a* concentrations are highly uncertain in the Southern Ocean (e.g., Dierssen and Smith, 2000; Hirawake et al., 2000; Johnson et al., 2013). Hirawake et al. (2011) proposed a new PP_{eu} algorithm based on phytoplankton light absorption (an absorption-based algorithm) that does not use chl *a* concentration, and found that satellite PP_{eu} values derived from the Sea-viewing Wide

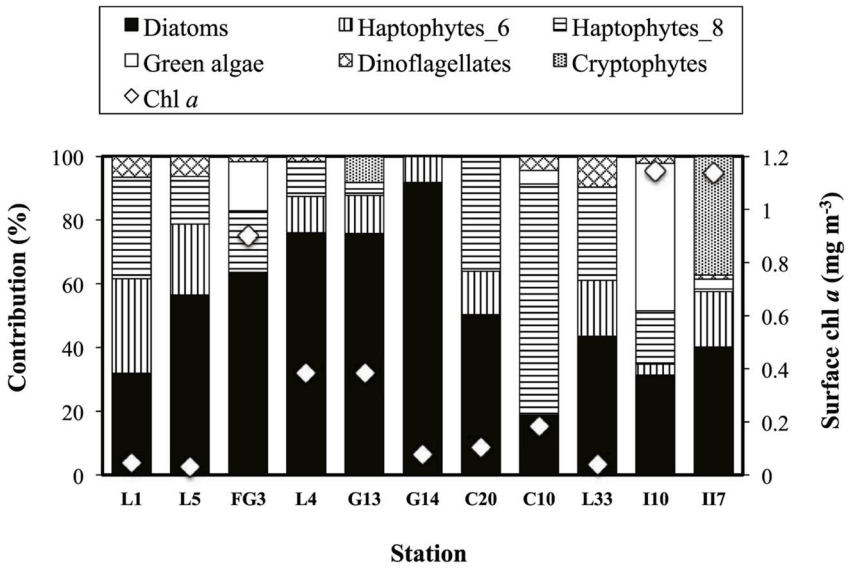

Fig. 4. Contributions of each algal class to total chl *a* biomass in the surface waters of the SACCZ as estimated using CHEMTAX. Note: the common name "Green algae" includes Chlorophyceae, Prasinophyceae, and may include Euglenophyceae.

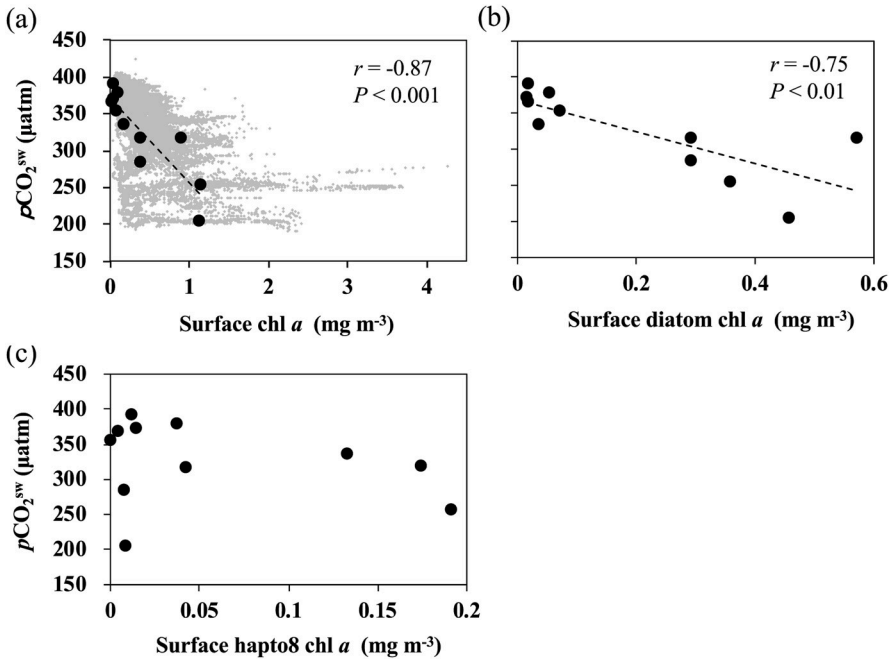

Fig. 5. Relationships between pCO_2^{sw} and chl *a* concentration for (a) total phytoplankton, (b) diatoms, and (c) type 8 haptophytes. The gray dots represent the relationship between pCO_2^{sw} and chl *a* concentration estimated from the fluorescence sensor along the cruise tracks in the region south of 60°S. The dashed line in each figure represents the regression line, which had statistical significance at the 95% confidence level. These statistics are shown in Table 2.

Field-of-view Sensor (SeaWiFS) were in better agreement with in situ values than previous chl *a*-based algorithms in the Indian sector of the Southern Ocean (Hirawake et al., 2011; Takao et al., 2012).

Our results suggest that the distribution of pCO_2^{sw} during austral summer in the study region can be estimated using chl *a* concentration and PP_{eu} values (Figs. 5 and 6 and Tables 2 and 3). In this study, to determine the mean pCO_2^{sw} distribution in the Indian sector of the Southern Ocean, we employed satellite PP_{eu} and chl *a* images with 9-km spatial resolution derived from the SeaWiFS, which was determined with the absorption-based algorithm by Hirawake et al. (2011) and the OCI algorithm by Hu et al. (2012), respectively. In this study, the reconstructions of pCO_2 distribution were restricted to the period 1997/1998–2006/2007 due to the use of satellite PP_{eu} and chl *a* values derived from SeaWiFS.

Fig. 7 shows the climatological satellite-derived PP_{eu} distribution in our study region during the austral summer (December–February) from 1997/1998–2006/2007. The climatological satellite pCO_2^{sw} distribution during the austral summer was estimated using pCO_2^{sw} data corrected to the reference year 2000 (Fig. 8a and S2), with an expected annual pCO_2^{sw} increase of about 2.0 µatm per year (Metzl, 2009), and the climatological map was compared with that of Takahashi et al. (2009, hereafter referred as to T09). Although the climatological map of T09 was constructed using pCO_2^{sw} values obtained from 1970 to 2007, data collected before 1996 in the Indian sector of the Southern Ocean is very limited (Takahashi et al., 1997, 2002). The longitudinal distribution of climatological mean pCO_2^{sw} during the austral summer averaged over 55–65°S

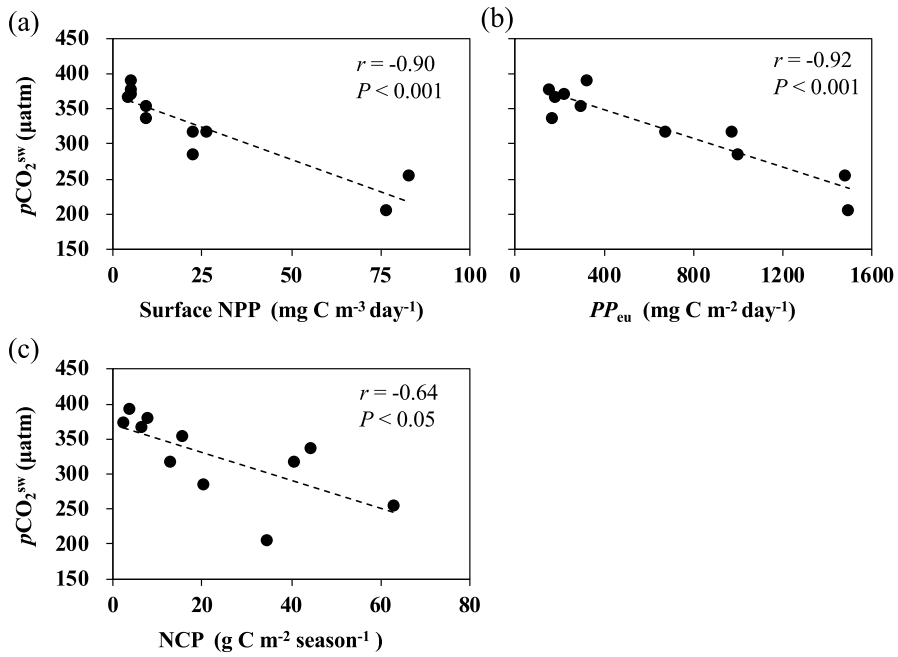

Fig. 6. Relationships of pCO_2^{sw} with (a) surface NPP and (b) depth-integrated NPP within the euphotic layer (PP_{eu}) for total phytoplankton, and with (c) seasonally integrated net community production (NCP). The dashed line in each figure represents the regression line, which had statistical significance at the 95% confidence level. These statistics are shown in Table 3.

Table 2
Coefficients of regression for the relationships between pCO_2^{sw} and chl *a* concentrations derived from total phytoplankton, diatoms, or type 8 haptophytes.

	Slope ± S.E.	Intercept ± S.E.	*r*	*P*	*n*
All	**−114.8 ± 20.1**	**371.2 ± 11.8**	**−0.87**	**<0.001**	11
Diatoms	**−220.7 ± 59.1**	**368.4 ± 16.4**	**−0.75**	**<0.01**	11
Type 8 haptophytes	−231.7 ± 256.1	337.7 ± 22.6	−0.13	0.39	11

Bold numbers denote statistical significance at the 95% confidence level ($P < 0.05$).

agreed with that of T09, although the minimum pCO_2^{sw} value was observed in the area west of 90°E in our results (Figs. 8 and 9, S2 and S3). These results suggest that the pCO_2^{sw} distribution could be estimated at high spatial resolution using the simplified relationship proposed here; however, the applicable period of ocean color data is limited to austral summer, when phytoplankton productivity is enhanced.

For the period 1997/1998–2006/2007 during the austral summer (December–February), the root mean squared error (RMSE) between monthly mean pCO_2^{sw} estimated from satellite PP_{eu} with 9-km spatial resolution and in situ pCO_2^{sw} along cruise tracks for SOCAT version 2019 (Table S1) was 29.3 µatm (n = 5598; Fig. S4), which is relatively high to RMSE for a combined approach of a self-organizing map and feed-forward neural network (ETH-SOMFFN) reported by Landschützer et al. (2015) for the entire Southern Ocean (i.e., the region south of 35°S) and all seasons (apporox. 20 µatm for SOCAT and 25 µatm for LDEO). This could be due to limitations of spaciotemporal scale for our pCO_2^{sw} estimates (i.e., the region south of 55°S and austral summer only) and properties of our model based on biological process without consideration of other effects, such as changes in water temperature and salinity.

Table 3
Coefficients of regression for the relationships of pCO_2^{sw} with surface NPP and depth-integrated NPP within the euphotic layer (PP_{eu}) for total phytoplankton.

	Slope ± S.E.	Intercept ± S.E.	*r*	*P*	*n*
Surface	**−1.8 ± 0.3**	**369.8 ± 10.3**	**−0.90**	**<0.001**	11
Depth-integrated	**−0.1 ± 0.0**	**389.8 ± 11.2**	**−0.92**	**<0.001**	11

Bold numbers denote statistical significance at the 95% confidence level ($P < 0.05$).

3.5. Interannual variations in pCO_2^{sw} and air-sea exchange of CO_2

Several pCO_2 mapping methods have been developed to estimate the spatiotemporal variations in pCO_2^{sw} and air-sea exchange of CO_2 using in situ pCO_2 databases, at both regional and global scales (e.g., Landschützer et al., 2015; Rödenbeck et al., 2015). In this study, we propose a novel approach to estimate spatiotemporal variations in pCO_2^{sw} in the Southern Ocean using satellite PP_{eu} images. Fig. 10 shows interannual

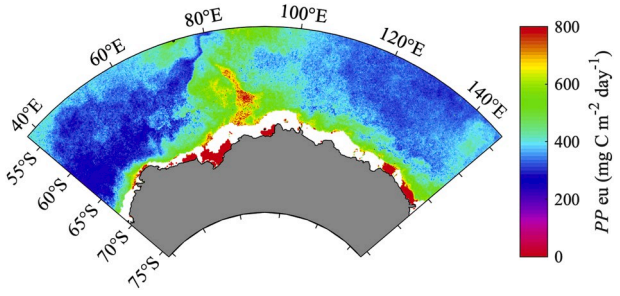

Fig. 7. Climatological satellite-derived PP_{eu} distribution during the austral summer (December–February) from 1997/1998 to 2006/2007, which was reported by Takao et al. (2012). White areas represent no satellite data due to cloudiness or sea ice cover.

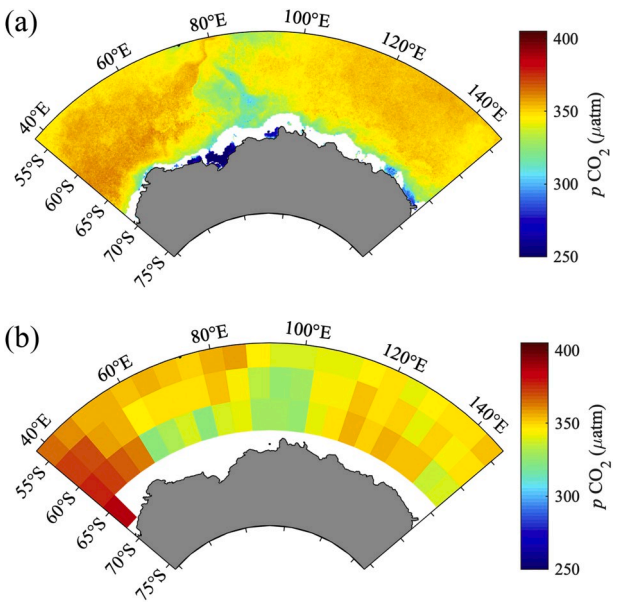

Fig. 8. Climatological mean pCO_2^{sw} distributions during the austral summer derived from (a) satellite PP_{eu} images from 1997/1998–2006/2007 (Takao et al., 2012) and (b) values reported by Takahashi et al. (2009). White areas in upper figure represent no satellite data due to cloudiness or sea ice cover.

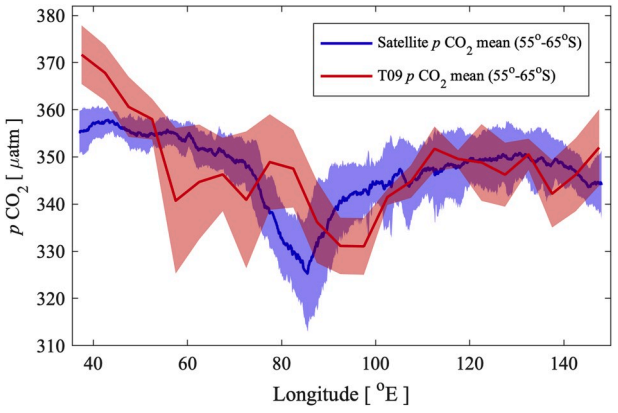

Fig. 9. Comparison of the longitudinal distribution of the climatological mean pCO_2^{sw} averaged over 55–65°S during austral summer (December–February) with that derived from satellite PP_{eu} images and that reported by Takahashi et al. (2009) (T09). The blue or red solid lines and shaded areas denote the mean values and standard deviations, respectively, of satellite and T09 pCO_2^{sw} values in the area. (For interpretation of the references to color in this figure legend, the reader is referred to the Web version of this article.)

variations in the longitudinal distribution of reconstructed pCO_2^{sw} averaged over the region south of 55°S during the austral summer (December–February). The longitudinal pCO_2^{sw} distribution based on satellite PP_{eu} values was compared with that based on ETH-SOMFFN (Landschützer et al., 2017). Our longitudinal pCO_2^{sw} distribution was consistent with that from ETH-SOMFFN, despite being obtained using different mapping methods and datasets. This complementarity supports the robustness of our method for assessing air-sea exchange of CO_2 in the Southern Ocean. In some years, pCO_2^{sw} distributions for ETH-SOMFFN were higher than our results (i.e., the period 2006–2007). For this period, SOCAT data had relatively low pCO_2^{sw} levels in the area from 80° to 130°E around 65°S (Fig. 1), and our results better reproduced SOCAT data than ETH-SOMFFN (Fig. 10). For the period 2000–2001, in contrast, the ETH-SOMFFN model relatively well reproduced high pCO_2^{sw} levels in the area from 80° to 100°E, which was not reproduced in our result. In this region, lower PP_{eu} values were observed in the period 2000–2001 (Fig. S5), and physical process such as upwelling/deep mixing, which enhances a vertical transport of DIC-rich subsurface waters from the deep ocean (e.g., Shim et al., 2006), would be more dominant than biological process. The pCO_2^{sw} for ETH-SOMFFN was developed using SOCAT version 4 (Landschützer et al., 2017), which did not include the relatively low pCO_2^{sw} data for the zone 30° to 70°E reported by Roden et al. (2016) as well as our data. Thus, relatively high pCO_2^{sw} levels for ETH-SOMFFN could be due to the pCO_2^{sw} dataset used for the model development.

Integrated air-sea CO_2 flux (FCO_2) over the study region was calculated using the following equation:

$$FCO_2 = k \times s\,(pCO_2^{air} - pCO_2^{sw}) \times (100/A) \times 100 \quad (2)$$

$$k = (0.029u^3 + 5.4) \times (660/\mathrm{Sc})^{0.5} \quad (3)$$

where k is the CO_2 gas transfer coefficient (Edson et al., 2011); s is the solubility of CO_2 in seawater, which is a function of temperature and salinity (Weiss, 1974); A is the sea ice concentration; u is wind speed from NCEP (National Centers for Environmental Prediction) reanalysis monthly data; and Sc is the Schmidt number of CO_2 (Wanninkhof, 1992). Monthly mean sea surface temperature and sea ice concentration data were obtained from the NOAA Optimum Interpolation Sea Surface Temperature V2 database (https://www.esrl.noaa.gov/psd/data/gridded/data.noaa.oisst.v2.html), and monthly mean sea surface salinity values were taken from the World Ocean Atlas (https://www.nodc.noaa.gov/OC5/woa13/woa13data.html). Monthly mean pCO_2^{air} distributions in our study region during the austral summer from 1997/1998–2006/2007 were obtained from climatological pCO_2^{air} data (Takahashi et al., 2009), and accounted for the expected annual increase of 1.7 μatm per year (Metzl, 2009). Monthly mean pCO_2^{sw} distributions were estimated based on satellite PP_{eu} and ETH-SOMFFN shown in Fig. 10.

Estimated climatological FCO_2 integrated over the region south of 55°S derived from satellite PP_{eu} and chl a images during the austral summer was −11.2 and −11.8 Tg C per season, respectively, which is comparable to the climatological value (−10.9 Tg C per season) reported previously for the same region (Takahashi et al., 2009). Interannual variations in integrated FCO_2 over the study region from 1997/1998–2006/2007 are shown in Fig. 11, and integrated FCO_2 ranged from −23.5 Tg C per season in 2006/2007 to 1.8 Tg C per season in 1997/1998. A strong sink of CO_2 in 1999/2000 and 2006/2007 would be due to relatively high PP_{eu} in the study region, mainly the eastern areas compared to other years (Fig. 11 and S5). In this period, wind speeds were also relatively strong in the study region. This enhanced PP_{eu} with increasing wind speeds could possibly be related to the regional-specific climatic variations such as SAM in the marginal ice zone (e.g., Johnston and Gabric, 2011; Lovenduski and Gruber, 2005). A significant positive correlation was found between the SAM index and the integrated PP_{eu} ($r = 0.65$, $P < 0.05$, $n = 10$) and the averaged wind speed ($r = 0.87$, $P < 0.001$, $n = 10$) over the study region (Fig. S6). This enhanced PP_{eu} with increasing wind speeds could be due to changes in sea ice and meltwater dynamics (i.e., changes in light and/or iron availability), driven by enhanced westerly winds in positive phases of the SAM (e.g., Doddridge and Marshall, 2017).

Although no significant trends were found in integrated FCO_2 from 1997/1998–2006/2007 due to a sharp decline in 1999/2000, a statistically significant reduction was found from 2000/2001–2006/2007, with an annual decrease rate of 2.6 Tg C per year ($P < 0.05$). A similar reduction was found using integrated FCO_2 based on ETH-SOMFFN (Landschützer et al., 2017). The increasing oceanic CO_2 uptake over 2000/2001–2006/2007 was consistent with other estimates in the Southern Ocean (e.g., Fay et al., 2018), although their study area was different from this study. These independent results support the conclusion that the Southern Ocean CO_2 sink was increasing in the 2000s (Landschützer et al., 2015).

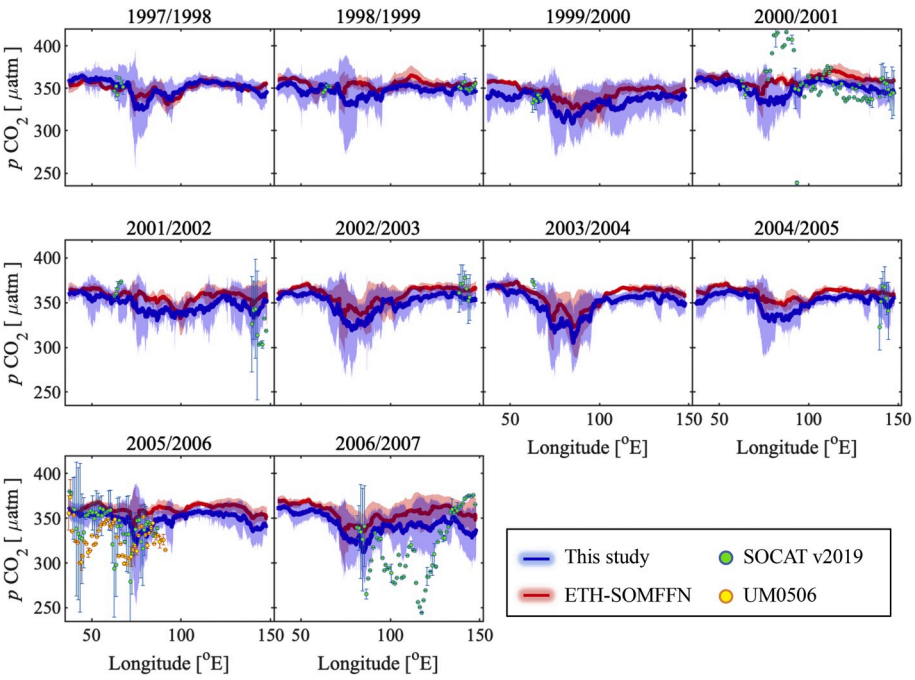

Fig. 10. Interannual variations of the longitudinal distribution of reconstructed pCO_2^{sw} averaged over the region south of 55°S during austral summer. The blue or red solid lines and shaded areas denote the mean values and the standard deviations, respectively, of pCO_2^{sw} based on satellite imagery and a combined approach using self-organizing maps and feed-forward neural networks (ETH-SOMFFN; Landschützer et al., 2017) in the study area. Green and yellow circles denote the mean values and the standard deviations of the in situ pCO_2^{sw} values obtained from SOCAT version 2019 (Bakker et al., 2016) and the UM0506 underway measurement, respectively. Sea surface fCO_2 values from SOCAT were used as pCO_2^{sw}. (For interpretation of the references to color in this figure legend, the reader is referred to the Web version of this article.)

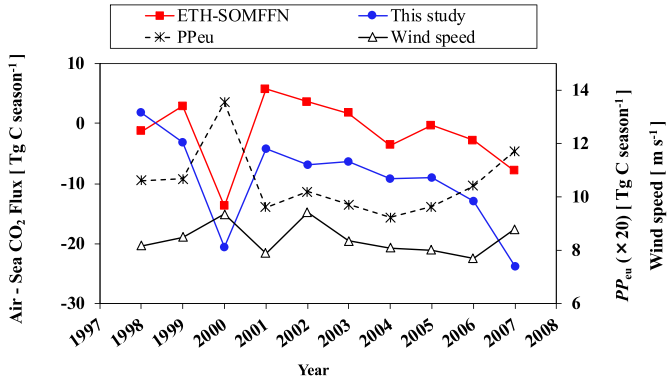

Fig. 11. Inter-annual variation of the integrated FCO_2 over the study region (Tg C per season) from 1997/1998–2006/2007 during the austral summer. The blue dot and red square denote the variations of the integrated FCO_2 based on satellite PP_{eu} and ETH-SOMFFN, respectively. The asterisk and open triangle denote the integrated PP_{eu} and the averaged wind speed over the study region, respectively. (For interpretation of the references to color in this figure legend, the reader is referred to the Web version of this article.)

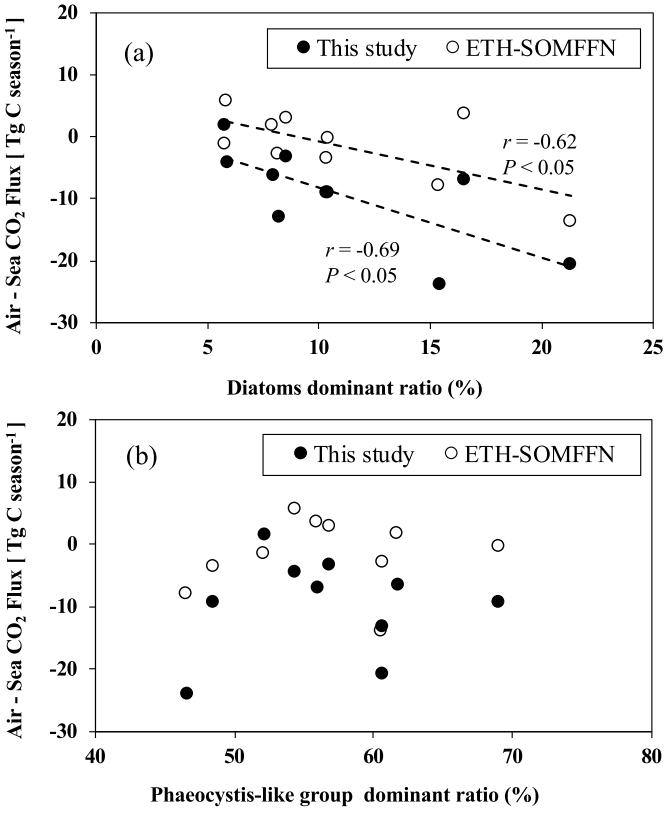

Fig. 12. Relationships between integrated FCO_2 and satellite-derived dominance ratio of (a) diatoms and (b) *Phaeocystis*-like (i.e., type 8 haptophytes) phytoplankton in the study region. The dashed line in each figure represents the regression line, which had statistical significance at the 95% confidence level.

To assess the impact of changes in phytoplankton community on this trend, we investigated the relationships between integrated FCO_2 and satellite-derived dominance ratios of diatoms and *Phaeocystis*-like (i.e., type 8 haptophytes) phytoplankton (Alvain et al., 2005, 2008; Ben Mustapha et al., 2014) over the region south of 55°S in the Indian sector of the Southern Ocean (Fig. 12). These ratios were calculated from the number of pixels where each phytoplankton community (e.g., diatoms) is dominant; the sum of the number of pixels for each dominant phytoplankton community was recorded, including nanoplankton-sized autotrophic flagellates (nanoflagellates), *Prochlorococcus*, *Synechococcus*, diatoms, and *Phaeocystis*-like phytoplankton (for more details, see Takao et al., 2012). Over the period from 1997 to 2007, integrated FCO_2 during austral summer based on satellite remote sensing and ETH-SOMFFN was negatively correlated with the dominance ratio of diatoms, but not correlated with the *Phaeocystis*-like group. The negative correlation between variations in FCO_2 and diatoms was consistent with the observations described in section 3.2 and in previous studies (Brown et al., 2019; Moreau et al., 2012, 2013), although these observations were based on pCO_2^{sw} or ΔpCO_2. Several studies reported the predominance of *Phaeocystis*-like phytoplankton in regions of deep mixed layers in the Southern Ocean (e.g., Alvain et al., 2008; Arrigo et al., 1999).

Mixing process would enhance a vertical transport of CO_2-rich waters from the deep ocean (e.g., Shim et al., 2006), and such physical processes may control CO_2 dynamics rather than biological processes in regions where *Phaeocystis*-like phytoplankton dominated. Our results suggest that a future shift in the dominant phytoplankton community from diatoms to another group due to climate change (e.g., Deppeler and Davidson, 2017) may have major implications for the carbon cycle of the Southern Ocean, causing changes in air-sea exchange of CO_2 in this region, as recently shown by the enhanced oceanic CO_2 uptake over the past 25 years with shifts in phytoplankton community composition (i.e., an increase in diatoms) along the WAP (i.e., Brown et al., 2019).

4. Conclusions

This study describes changes in the abundance of phytoplankton groups determined from pigment signatures and NPP and their effects on variations in pCO_2^{sw} in the Indian sector of the Southern Ocean. We found that pCO_2^{sw} in the SACCZ during our cruises was negatively correlated with chl *a* concentrations derived from total phytoplankton or diatoms, but not correlated with that of type 8 haptophytes (presumably *P. antarctica*). Furthermore, strong correlations were found between pCO_2^{sw} and NPP. These results suggest that changes in the dominant phytoplankton group and productivity may control CO_2 dynamics in the marginal ice zone of the Indian sector of the Southern Ocean, along with changes in physical processes such as thermodynamics, air-sea exchange of CO_2, and horizontal and vertical advection of water masses. We also estimated the climatological mean pCO_2^{sw} during austral summer using satellite images and the empirical relationship between pCO_2^{sw} and PP_{eu} (or chl *a* concentrations). Over the period from 1997 to 2007, the integrated FCO_2 over the study region showed very large variations from a small source in 1997/1998, a strong sink in 1999/2000 and 2006/2007, and a progressive increasing sink was found from 2000/2001–2006/2007. We found very coherent results with other methods, but the use of satellite PP_{eu} to reconstruct pCO_2^{sw} and FCO_2 in the Southern Ocean is at present limited to the summer season. Previous studies suggest that the effects of phytoplankton community composition on CO_2 dynamics may differ spatiotemporally within the Southern Ocean (e.g., the WAP and the Weddell Sea). Thus, further studies examining the relationship between pCO_2^{sw} and phytoplankton community composition in the Southern Ocean are needed.

Declaration of competing interest

The authors declare that they have no known competing financial interests or personal relationships that could have appeared to influence the work reported in this paper.

Acknowledgments

We are grateful to the captain and crew of the TR/V *Umitaka-Maru*, Dr. M. Moteki (Tokyo University of Marine Science and Technology), and many other colleagues onboard for their assistance with sample collection during the cruises. We thank the Distributed Active Archive Center at the Goddard Space Flight Center for the production and distribution of satellite data. We also thank the Surface Ocean CO_2 Atlas (SOCAT), which is an international effort, endorsed by the International Ocean Carbon Coordination Project (IOCCP), the Surface Ocean Lower Atmosphere Study (SOLAS) and the Integrated Marine Biosphere Research (IMBeR) program, to deliver a uniformly quality-controlled surface ocean CO_2 database. The many researchers and funding agencies responsible for the collection of data and quality control are thanked for their contributions to SOCAT. We also thank Dr. T. Odate (National Institute of Polar Research) for the opportunity to join the Japanese Antarctic Research Expedition (JARE) program. Finally, we appreciate the editor, Dr. Sébastien Moreau, and an anonymous reviewer for providing valuable comments that improved the manuscript significantly. This work was supported in part by the Japan Society for the Promotion of Science (JSPS) KAKENHI Grant Numbers JP17H06319 and JP19K20445, JARE programs, and the NIES Low-Carbon Research Program.

Appendix A. Supplementary data

Supplementary data to this article can be found online at https://doi.org/10.1016/j.dsr.2020.103263.

References

Alvain, S., Moulin, C., Dandonneau, Y., Breon, F.M., 2005. Remote sensing of phytoplankton groups in case 1 waters from global SeaWiFS imagery. Deep-Sea Res. I 52, 1989–2004.

Alvain, S., Moulin, C., Dandonneau, Y., Loisel, H., 2008. Seasonal distribution and succession of dominant phytoplankton groups in the global ocean: a satellite view. Global Biogeochem. Cycles 22, GB3001. https://doi.org/10.1029/2007GB003154.

Alvain, S., Le Quéré, C., Bopp, L., Racault, M.F., Beaugrand, G., Dessailly, D., Buitenhuis, E.T., 2013. Rapid climatic driven shifts of diatoms at high latitudes. Remote Sens. Environ. 132, 195–201.

Armstrong, R.A., Lee, C., Hedges, J.I., Honjo, S., Wakeham, A.G., 2002. A new, mechanistic model for organic carbon fluxes in the ocean based on the quantitative association of POC with ballast minerals. Deep-Sea Res. II 49, 219–236.

Arrigo, K.R., Robinson, D.H., Worthen, D.L., Dunbar, R.B., DiTullio, G.R., van Woert, M., Lizotte, M.P., 1999. Phytoplankton community structure and the drawdown of nutrients and CO_2 in the Southern Ocean. Science 283, 365–367.

Bakker, D.C.E., Pfeil, B., Landa, C.S., Metzl, N., O'Brien, K.M., Olsen, A., Smith, K., Cosca, C., Harasawa, S., Jones, S.D., Nakaoka, S., Nojiri, Y., Schuster, U., Steinhoff, T., Sweeney, C., Takahashi, T., Tilbrook, B., Wada, C., Wanninkhof, R., Alin, S.R., Balestrini, C.F., Barbero, L., Bates, N.R., Bianchi, A.A., Bonou, F., Boutin, J., Bozec, Y., Burger, E.F., Cai, W.-J., Castle, R.D., Chen, L., Chierici, M., Currie, K., Evans, W., Featherstone, C., Feely, R.A., Fransson, A., Goyet, C., Greenwood, N., Gregor, L., Hankin, S., Hardman-Mountford, N.J., Harlay, J., Hauck, J., Hoppema, M., Humphreys, M.P., Hunt, C.W., Huss, B., Ibánhez, J.S.P., Johannessen, T., Keeling, R., Kitidis, V., Körtzinger, A., Kozyr, A., Krasakopoulou, E., Kuwata, A., Landschützer, P., Lauvset, S.K., Lefèvre, N., Monaco, C.L., Manke, A., Mathis, J.T., Merlivat, L., Millero, F.J., Monteiro, P.M.S., Munro, D.R., Murata, A., Newberger, T., Omar, A.M., Ono, T., Paterson, K., Pearce, D., Pierrot, D., Robbins, L. L., Saito, S., Salisbury, J., Schlitzer, R., Schneider, B., Schweitzer, R., Sieger, R., Skjelvan, I., Sullivan, K.F., Sutherland, S.C., Sutton, A.J., Tadokoro, K., Telszewski, M., Tuma, M., Van Heuven, S.M.A.C., Vandemark, D., Ward, B., Watson, A.J., Xu, S., 2016. A multi-decade record of high-quality fCO_2 data in version 3 of the Surface Ocean CO_2 Atlas (SOCAT). Earth Syst. Sci. Data 8, 383–413. https://doi.org/10.5194/essd-8-383-2016.

Ben Mustapha, Z., Alvain, S., Jamet, C., Loisel, H., Dessailly, D., 2014. Automatic classification of water-leaving radiance anomalies from global SeaWiFS imagery: application to the detection of phytoplankton groups in open ocean waters. Remote Sens. Environ. 146, 97–112.

Brown, M.S., Munro, D.R., Feehan, C.J., Sweeney, C., Ducklow, H.W., Schofield, O.M., 2019. Enhanced oceanic CO_2 uptake along the rapidly changing West Antarctic Peninsula. Nat. Clim. Change 9, 678–683. https://doi.org/10.1038/s41558-019-0552-3.

Buitenhuis, E., van der Wal, P., de Baar, H., 2001. Blooms of Emiliania huxleyi are sinks of atmospheric carbon dioxide: a field and mesocosm study derived simulation. Global Biogeochem. Cycles 15, 577–587. https://doi.org/10.1029/2000GB001292.

Carrillo, C.J., Smith, R.C., Karl, D.M., 2004. Processes regulating oxygen and carbon dioxide in surface waters west of the Antarctic Peninsula. Mar. Chem. 84, 161–179.

Codispoti, L.A., Friedrich, G.E., Hood, D.W., 1986. Variability in the inorganic carbon system over the southeastern Bering Sea shelf during spring 1980 and spring-summer 1981. Continent. Shelf Res. 5, 133–160.

Copin-Montégut, C., 1988. A new formula for the effect of temperature on the partial pressure of CO_2 in seawater. Mar. Chem. 25, 29–37.

Copin-Montégut, C., 1989. A new formula for the effect of temperature on the partial pressure of CO_2 in seawater. Corrigendum. Mar. Chem. 27, 143–144.

de Boyer Montégut, C., Madec, G., Fischer, A.S., Lazar, A., Iudicone, D., 2004. Mixed layer depth over the global ocean: an examination of profile data and a profile-based climatology. J. Geophys. Res. 109, C12003 https://doi.org/10.1029/2004JC002378.

Deppeler, S.L., Davidson, A.T., 2017. Southern Ocean phytoplankton in a changing climate. Front. Mar. Sci. 4 https://doi.org/10.3389/fmars.2017.00040.

Dierssen, H.M., Smith, R.C., 2000. Bio-optical properties and remote sensing ocean color algorithms for Antarctic Peninsula waters. J. Geophys. Res. 105, 26301–26312. https://doi.org/10.1029/1999JC000296.

DiTullio, G.R., Grebmeier, J.M., Arrigo, K.R., Lizotte, M.P., Robinson, D.H., Leventer, A., Barry, J.P., VanWoert, M.L., Dunbar, R.B., 2000. Rapid and early export of *Phaeocystis antarctica* blooms in the Ross Sea, Antarctica. Nature 404, 595–598.

Doddridge, E.W., Marshall, J., 2017. Modulation of the seasonal cycle of Antarctic sea ice extent related to the Southern Annular Mode. Geophys. Res. Lett. 44, 9761–9768.

Dong, S., Sprintall, J., Gille, S.T., Talley, L., 2008. Southern Ocean mixed-layer depth from Argo float profiles. J. Geophys. Res. 113, C06013 https://doi.org/10.1029/2006JC004051.

Edson, J.B., Fairall, C.W., Bariteau, L., Zappa, C.J., Cifuentes-Lorenzen, A., McGillis, W. R., Pezoa, S., Hare, J.E., Helmig, D., 2011. Direct covariance measurement of CO_2 gas transfer velocity during the 2008 Southern Ocean Gas Exchange Experiment: wind speed dependency. J. Geophys. Res. 116, C00F10 https://doi.org/10.1029/2011JC007022.

Fay, A.R., Lovenduski, N.S., McKinley, G.A., Munro, D.R., Sweeney, C., Gray, A.R., Landschützer, P., Stephens, B.B., Takahashi, T., Williams, N., 2018. Utilizing the drake passage time-series to understand variability and change in subpolar Southern Ocean pCO_2. Biogeosciences 15, 3841–3855.

Frankignoulle, M., Canon, C., Gattuso, J.-P., 1994. Marine calcification as a source of carbon dioxide: positive feedback of increasing atmospheric CO_2. Limnol. Oceanogr. 39, 458–462.

Garcia, H.E., Locarnini, R.A., Boyer, T.P., Antonov, J.I., Baranova, O.K., Zweng, M.M., Reagan, J.R., Johnson, D.R., 2014. In: Levitus, S., Mishonov Technical, A. (Eds.), World Ocean Atlas 2013, Volume 4: Dissolved Inorganic Nutrients (Phosphate, Nitrate, Silicate), p. 25. NOAA Atlas NESDIS 76.

Goldman, J.A.L., Kranz, S.A., Young, J.N., Tortell, P.D., Stanley, R.H.S., Bender, M.L., Morel, F.M.M., 2015. Gross and net production during the spring bloom along the Western Antarctic Peninsula. New Phytol. 205, 182–191. https://doi.org/10.1111/nph.13125.

Gruber, N., Gloor, M., Mikaloff Fletcher, S.E., Doney, S.C., Dutkiewicz, S., Follows, M.J., Gerber, M., Jacobson, A.R., Joos, F., Lindsay, K., Menemenlis, D., Mouchet, A., Müller, S.A., Sarmiento, J.L., Takahashi, T., 2009. Oceanic sources, sinks, and transport of atmospheric CO_2. Global Biogeochem. Cycles 23, GB1005. https://doi.org/10.1029/2008GB003349.

Hama, T., Miyazaki, T., Ogawa, Y., Iwakuma, T., Takahashi, M., Otsuki, A., Ichimura, S., 1983. Measurement of photosynthetic production of a marine phytoplankton population using a stable ^{13}C isotope. Mar. Biol. 73, 31–36.

Hashihama, F., Hirawake, T., Kudoh, S., Kanda, J., Furuya, K., Yamaguchi, Y., Ishimaru, T., 2008. Size fraction and class composition of phytoplankton in the Antarctic marginal ice zone along the 140°E meridian during February–March 2003. Pol. Sci. 2, 109–120.

Hirawake, T., Satoh, H., Ishimaru, T., Yamaguchi, Y., Kishino, M., 2000. Bio-optical relationship of Case I waters: the difference between the low- and mid-latitude waters and the Southern Ocean. J. Oceanogr. 56, 245–260.

Hirawake, T., Takao, S., Horimoto, N., Ishimaru, T., Yamaguchi, Y., Fukuchi, M., 2011. A phytoplankton absorption-based primary productivity model for remote sensing in the Southern Ocean. Polar Biol. 34, 291–302.

Hoppema, M., Fahrbach, E., Stoll, M.H.C., de Baar, H.J.W., 1999. Annual uptake of atmospheric CO_2 by the Weddell Sea derived from a surface layer balance, including estimations of entrainment and new production. J. Mar. Syst. 19, 219–233.

Hu, C., Lee, Z., Franz, B., 2012. Chlorophyll *a* algorithms for oligotrophic oceans: a novel approach based on three-band reflectance difference. J. Geophys. Res. 117, C01011 https://doi.org/10.1029/2011JC007395.

Inoue, Y.H., Matsueda, H., Ishii, M., Fushimi, K., Hirota, M., Asanuma, I., Takasugi, Y., 1995. Long-term trend of the partial pressure of carbon dioxide (pCO_2) in surface waters of the western North Pacific, 1984–1993. Tellus 47B, 391–413.

Inoue, Y.H., Ishii, M., Matsueda, H., Saito, S., Midorikawa, T., Nemoto, K., 1999. MRI measurements of partial pressure of CO_2 in surface waters of the Pacific during 1968 to 1970: re-evaluation and comparison of data with those of the 1980s and 1990s. Tellus 51B, 830–848.

Ito, T., Woloszyn, M., Mazloff, M., 2010. Anthropogenic carbon dioxide transport in the Southern Ocean driven by Ekman flow. Nature 463, 80–83.

Ishii, M., Inoue, Y.H., Matsueda, H., Tanoue, E., 1998. Close coupling between seasonal biological production and dynamics of dissolved inorganic carbon in the Indian Ocean sector and the Western Pacific Ocean sector of the Antarctic Ocean. Deep-Sea Res. I 45, 1187–1209.

Ishii, M., Inoue, Y.H., Matsueda, H., 2002. Net community production in the marginal ice zone and its importance of the variability of oceanic pCO_2 in the Southern Ocean south of Australia. Deep-Sea Res. II 49, 1691–1706.

Jabaud-Jan, A., Metzl, N., Brunet, C., Poisson, A., Schauer, B., 2004. Interannual variability of the carbon dioxide system in the southern Indian Ocean (20°S–60°S): the impact of a warm anomaly in austral summer 1998. Global Biogeochem. Cycles 18, GB1042. https://doi.org/10.1029/2002GB002017.

Jennings, J.C., Gordon, L.I., Nelson, D.M., 1984. Nutrient depletion indicates high primary productivity in the Weddell Sea. Nature 309, 51–54.

Johnson, R., Strutton, P.G., Wright, S.W., McMinn, A., Meiners, K.M., 2013. Three improved satellite chlorophyll algorithms for the Southern Ocean. J. Geophys. Res. 118 https://doi.org/10.1002/jgrc.20270.

Johnston, B.M., Gabric, A.J., 2011. Interannual variability in estimated biological productivity in the Australian sector of the Southern Ocean in 1997–2007. Tellus 63B, 266–286.

Khatiwala, S., Primeau, F., Hall, T., 2009. Reconstruction of the history of anthropogenic CO_2 concentrations in the ocean. Nature 462, 346–349.

Landschützer, P., Gruber, N., Haumann, F.A., Rödenbeck, C., Bakker, D.C.E., van Heuven, S., Hoppema, M., Metzl, N., Sweeney, C., Takahashi, T., Tilbrook, B., Wanninkhof, R., 2015. The reinvigoration of the Southern Ocean carbon sink. Science 349, 1221–1224.

Landschützer, P., Gruber, N., Bakker, D.C.E., 2017. An Updated Observation-Based Global Monthly Gridded Sea Surface pCO_2 and Air-Sea CO_2 Flux Product from 1982 through 2015 and its Monthly Climatology (NCEI Accession 0160558). Version 2.2. NOAA National Centers for Environmental Information. Dataset., 2017-07-11.

Lenton, A., Tilbrook, B., Law, R.M., Bakker, D., Doney, S.C., Gruber, N., Ishii, M., Hoppema, M., Lovenduski, N.S., Matear, R.J., McNeil, B.I., Metzl, N., Mikaloff Fletcher, S.E., Monteiro, P.M.S., Rödenbeck, C., Sweeney, C., Takahashi, T., 2013. Sea–air CO_2 fluxes in the Southern Ocean for the period 1990–2009. Biogeosciences 10, 4037–4054.

Lovenduski, N.S., Gruber, N., 2005. Impact of the southern annular Mode on Southern Ocean circulation and biology. Geophys. Res. Lett. 32, L11603 https://doi.org/10.1029/2005GL022727.

Mackey, M.D., Mackey, D.J., Higgins, H.W., Wright, S.W., 1996. CHEMTAX-a program for estimating class abundances from chemical makers: application to HPLC measurements of phytoplankton. Mar. Ecol. Prog. Ser. 144, 265–283.

Marshall, G.J., 2003. Trends in the southern annular Mode from observations and reanalyses. J. Clim. 16, 4134–4143.

McNeil, B.I., Metzl, N., Key, R.M., Matear, R.J., Corbiere, A., 2007. An empirical estimate of the Southern Ocean air-sea CO_2 flux. Global Biogeochem. Cycles 21, GB3011. https://doi.org/10.1029/2007GB002991.

Metzl, N., 2009. Decadal increase of oceanic carbon dioxide in the Southern Indian Ocean surface waters (1991-2007). Deep-Sea Res. II 56, 607–619.

Metzl, N., Brunet, C., Jabaud-Jan, A., Poisson, A., Schauer, B., 2006. Summer and winter air–sea CO_2 fluxes in the Southern Ocean. Deep-Sea Res. I 53, 1548–1563.

Mikaloff Fletcher, S.E., Gruber, N., Jacobson, A.R., Doney, S.C., Dutkiewicz, S., Gerber, M., Follows, M., Joos, F., Lindsay, K., Menemenlis, D., Mouchet, A., Müller, S.A., Sarmiento, J.L., 2006. Inverse estimates of anthropogenic CO_2 uptake, transport, and storage by the ocean. Global Biogeochem. Cycles 20, GB2002. https://doi.org/10.1029/2005GB002530.

Minas, H.J., Minas, M., Packard, T.T., 1986. Productivity in upwelling areas deduced from hydrographic and chemical fields. Limnol. Oceanogr. 31, 1180–1204.

Moline, M.A., Claustre, H., Frazer, T.K., Schofield, O., Vernet, M., 2004. Alteration of the food web along the Antarctic Peninsula in response to a regional warming trend. Global Change Biol. 10, 1973–1980.

Montes-Hugo, M.A., Doney, S.C., Ducklow, H.W., Fraser, W., Martinson, D., Stammerjohn, S.E., Schofield, O., 2009. Recent changes in phytoplankton communities associated with rapid regional climate change along the Western Antarctic Peninsula. Science 323, 1470–1473.

Moreau, S., Schloss, I.R., Mostajir, B., Demers, S., Almandoz, G.O., Ferrario, M.E., Ferreyra, G.A., 2012. Influence of microbial community composition and metabolism on air−sea ΔpCO_2 variation off the western Antarctic Peninsula. Mar. Ecol. Prog. Ser. 446, 45–59.

Moreau, S., di Fiori, E., Schloss, I.R., Almandoz, G.O., Esteves, J.L., Paparazzo, F.E., Ferreyra, G.A., 2013. The role of phytoplankton community composition and microbial community metabolism in sea−air ΔpCO_2 variation in the Weddell Sea. Deep-Sea Res. I 82, 44–59.

Murphy, P.P., Nojiri, Y., Fujinuma, Y., Wong, C.S., Zeng, J., Kimoto, T., Kimoto, H., 2001. Measurements of surface seawater fCO_2 from volunteer commercial ships: techniques and experiences from *skaugran*. J. Atoms. Ocean Tech. 18, 1719–1734.

Nelson, D.M., Tréguer, P., Brzezinski, M.A., Leynaert, A., Quéguinet, B., 1995. Production and dissolution of biogenic silica in the ocean: revised global estimates, comparison with regional data and relationship to biogenic sedimentation. Global Biogeochem. Cycles 9, 359–372. https://doi.org/10.1029/95GB01070.

Nomura, D., Yoshikawa-Inoue, H., Kobayashi, S., Nakaoka, S., Nakata, K., Hashida, G., 2014. Winter-to-summer evolution of pCO_2 in surface water and air–sea CO_2 flux in the seasonal ice zone of the Southern Ocean. Biogeosciences 11, 5749–5761. https://doi.org/10.5194/bg-11-5749-2014.

Ono, T., Saino, T., Kurita, N., Sasaki, K., 2004. Basin-scale extrapolation of shipboard pCO2 data by using satellite SST and Chl *a*. Int. J. Rem. Sens. 25, 3803–3815.

Orsi, A.H., Wierderwohl, C.L., 2009. A recount of Ross Sea waters. Deep-Sea Res., II 56, 778–795.

Orsi, A.H., Whitworth III, T., Nowlin, W.D., 1995. On the meridional extent and fronts of the Antarctic Circumpolar Current. Deep-Sea Res. I 42, 641–673.

Redfield, A.C., Ketchum, B.H., Richard, F.A., 1963. The influence of organisms on the composition of sea-water. In: Hill, M.M. (Ed.), The Sea, vol. 2. Interscience, pp. 26–77.

Roden, N.P., Tilbrook, B., Trull, T.W., Virtue, P., Williams, G.D., 2016. Carbon cycling dynamics in the seasonal sea-ice zone of East Antarctica. J. Geophys. Res. 121, 8749–8769. https://doi.org/10.1002/2016JC012008.

Rödenbeck, C., Bakker, D.C.E., Gruber, N., Iida, Y., Jacobson, A.R., Jones, S., Landschützer, P., Metzl, N., Nakaoka, S., Olsen, A., Park, G.-H., Peylin, P., Rodgers, K.B., Sasse, T.P., Schuster, U., Shutler, J.D., Valsala, V., Wanninkhof, R., Zeng, J., 2015. Data-based estimates of the ocean carbon sink variability – first results of the Surface Ocean pCO_2 Mapping intercomparison (SOCOM). Biogeosciences 12, 7251–7278. https://doi.org/10.5194/bg-12-7251-2015.

Sarma, V.V.S.S., Saino, T., Sasaoka, K., Nojiri, Y., Ono, T., Ishii, M., Inoue, H.Y., Matsumoto, K., 2006. Basin-scale pCO2 distribution using satellite sea surface temperature, Chl *a*, and climatological salinity in the North Pacific in spring and summer. Global Biogeochem. Cycles 20. https://doi.org/10.1029/2005GB002594.

Schloss, I.R., Ferreyra, G.A., Ferrario, M.E., Almandoz, G.O., Codina, R., Alejandro, A., Balestrini, B., Ochoa, C.F., Pino, H.A., Poisson, A.D.R., 2007. Role of plankton communities in sea–air differences in pCO_2 in the SW Atlantic Ocean. Mar. Ecol. Prog. Ser. 332, 93–106.

Shadwick, E.H., Tilbrook, B., Cassar, N., Trull, T.W., Rintoul, S.R., 2015. Summertime physical and biological controls on O_2 and CO_2 in the Australian sector of the Southern Ocean. J. Mar. Syst. 147, 21–28.

Shim, J., Kang, Y.C., Kim, D., Choi, S., 2006. Distribution of net community production and surface pCO2 in the Scotia Sea, Antarctica, during austral spring 2001. Mar. Chem. 101, 68–84.

Stoll, M.H.C., Thomas, H., de Baar, H.J.W., Zondervan, I., de Jong, E., Bathmann, U.V., Fahrbach, E., 2002. Biological versus physical processes as drivers of large oscillations of the air–sea CO_2 flux in the Antarctic marginal ice zone during summer. Deep-Sea Res. II 49, 1651–1667.

Strutton, P.G., Griffiths, F.B., Waters, R.L., Wright, S.W., Bindoff, N.L., 2000. Primary productivity off the coast of the east Antarctica (80–150°E): january to march 1996. Deep-Sea Res. Pt. II 47, 2327–2362.

Sweeney, C., Smith, W.O., Hales, B., Bidigare, R.R., Carlson, C.A., Codispoti, L.A., Gordon, L.I., Hansell, D.A., Millero, F.J., Park, M.-O., Takahashi, T., 2000. Nutrient and carbon removal ratios and fluxes in the Ross Sea, Antarctica. Deep-Sea Res. II 47, 3395–3421.

Takahashi, T., Feely, R.A., Weiss, R., Wanninkhof, R.H., Chipman, D.W., Sutherland, S. C., Takahashi, T.T., 1997. Global air–sea flux of CO_2: an estimate basedon measurements of sea–air pCO_2 difference. Proc. Natl. Acad. Sci. Unit. States Am. 94, 8292–8299.

Takahashi, T., Sutherland, S.C., Sweeney, C., Poisson, A., Metzl, N., Tilbrook, B., Bates, N., Wanninkhof, R., Feely, R.A., Sabine, C., Olafsson, J., Nojiri, Y., 2002. Global sea–air CO2 flux based on climatological surface ocean pCO2, and seasonal biological and temperature effects. Deep-Sea Res. II 49, 1601–1622.

Takahashi, T., Sutherland, S.C., Wanninkhof, R., Sweeney, C., Feely, R.A., Chipman, D. W., Hales, B., Friederich, G., Chavez, F., Sabine, C., Watson, A., Bakker, D.C.E., Schuster, U., Metzl, N., Yoshikawa-Inoue, H., Ishii, M., Midorikawa, T., Nojiri, Y., Kortzinger, A., Steinhoff, T., Hoppema, M., Olafsson, J., Arnarson, T.S., Tilbrook, B., Johannessen, T., Olsen, A., Bellerby, R., Wong, C.S., Delille, B., Bates, N.R., de Baar, H.J.W., 2009. Climatological mean and decadal change in surface ocean pCO2 and net sea-air CO2 flux over the global oceans. Deep-Sea Res. II 56, 554–577.

Takahashi, T., Sweeney, C., Hales, B., Chipman, D.W., Newberger, T., Goddard, J.G., Iannuzzi, R.A., Sutherland, S.C., 2012. The changing carbon cycle in the Southern Ocean. Oceanography 25, 26–37.

Takao, S., Hirawake, T., Wright, S.W., Suzuki, K., 2012. Variations of net primary productivity and phytoplankton community composition in the Indian sector of the Southern Ocean as estimated from ocean-color remote sensing data. Biogeosciences 9, 3875–3890.

Tomczak, M., Liefrink, S., 2005. Interannual variations of water mass volumes in the Southern Ocean. J. Atmos. Ocean Sci. 10, 31–42.

Tréguer, P., Bowler, C., Moriceau, B., Dutkiewicz, S., Gehlen, M., Aumont, O., Bittner, L., Dugdale, R., Finkel, Z., Iudicone, D., Jahn, O., Guidi, L., Lasbleiz, M., Leblanc, K., Levy, M., Pondaven, P., 2018. Influence of diatom diversity on the ocean biological carbon pump. Nat. Geosci. 11, 27–37.

Tréguer, P., Pondaven, P., 2000. Silica control of carbon dioxide. Nature 406, 358–359.

Turner, J., Colwell, S.R., Marshall, G.J., Lachlan-Cope, T.A., Carleton, A.M., Jones, P.D., Lagun, V., Reid, P.A., Iagovkina, S., 2005. Antarctic climate change during the last 50 years. Int. J. Climatol. 25, 279–294.

Wanninkhof, R., 1992. Relationship between wind speed and gas exchange over the ocean. J. Geophys. Res. 97, 7373–7382.

Weiss, R.F., 1974. Carbon dioxide in water and seawater: the solubility of a non-ideal gas. Mar. Chem. 2, 203–215.

Welschmeyer, N.A., 1994. Fluorometric analysis of chlorophyll *a* in the presence of Chlorophyll *b* and pheopigments. Limnol. Oceanogr. 39, 1985–1992.

Westwood, K.J., Griffiths, F.B., Meiners, K.M., Williams, G.D., 2010. Primary productivity off the Antarctic coast from 30°–80°E; BROKE-West survey, 2006. Deep-Sea Res. Pt. II 57, 794–814.

Williams, G.D., Aoki, S., Jacobs, S.S., Rintoul, S.R., Tamura, T., Bindoff, N.L., 2010. Antarctic bottom water from the Adélie and George V land coast, east Antarctica (140–149°E). J. Geophys. Res. 115, C04027 https://doi.org/10.1029/2009JC005812.

Xu, S., Chen, L., Chen, H., Li, J., Lin, W., Qi, D., 2016. Sea-air CO2 fluxes in the Southern Ocean for the late spring and early summer in 2009. Remote Sens. Environ. 175, 158–166.

Yoshikawa, T., Meguro, M., Takeda, S., Furuya, K., 2007. Spatial heterogeneity in photosynthesis-irradiance parameters of phytoplankton across a cyclonic eddy in the Antarctic Divergence zone along 140°E. Geophys. Res. Lett. 34 https://doi.org/10.1029/2007GL030736.

Zapata, M., Jeffrey, S.W., Wright, S.W., Rodríguez, F., Garrido, J.L., Clementson, L., 2004. Photosynthetic pigments in 37 species (65 strains) of Haptophyta: implications for oceanography and chemotaxonomy. Mar. Ecol. Prog. Ser. 270, 83–102.